MeV X Rays and Photoneutrons from Femtosecond Laser-Produced Plasmas

H. Schwoerer,[1] P. Gibbon,[1] S. Düsterer,[1] R. Behrens,[1,2] C. Ziener,[1] C. Reich,[1] and R. Sauerbrey[1]

[1]*Institut für Optik und Quantenelektronik, Friedrich-Schiller-Universität, Max-Wien-Platz 1, 07743 Jena, Germany*
[2]*Physikalisch-Technische Bundesanstalt, Bundesallee 100, 38116 Braunschweig, Germany*

We demonstrate a novel method to monitor the total angular distribution of the spectrum of hard x-ray emission from a plasma generated with femtosecond laser pulses with an intensity of 5×10^{18} W/cm^2 on a solid target. Measured and calculated angular distributions of x rays show a pronounced anisotropy for MeV photon energies. We complemented the spectral information by demonstrating a (γ, n) nuclear reaction with a tabletop laser system.

PACS numbers: 52.27.Ny, 52.38.−r, 52.70.La

The interaction of an ultraintense femtosecond laser pulse with matter acts as a source of hot electrons, ions, and neutrons, as well as x rays of unique properties [1–5]: The duration of emission of both fast particles and short wavelength radiation is expected to be ultrashort, the area of the source is in the range of the laser focal spot size, and the emission becomes nonisotropic once the laser intensity exceeds 10^{18} W/cm^2, the intensity at which the generated hot electrons become relativistic [6,7]. These properties describe a source of excellent brightness, which may be used in subpicosecond time resolved diffraction experiments, imaging in ultrashort wavelength lithography, or to deliver ultrahigh radiation intensities for linear or even nonlinear x-ray-atom and x-ray-nuclei interactions.

One future application of ultrashort bunches of hot particles is the ignition of fusion in a precompressed pellet target [8]. This explains the tremendous theoretical and experimental efforts toward the generation of collimated particle beams with a well-known spectral shape. An even more visionary application of the emissions from femtosecond laser-produced plasmas is the transmutation of elements by proton interaction or neutron capture, such as deactivation of long-lived fission fragments or activation of short-lived isotopes used in radiological diagnostics and radiotherapy [9].

Beside these applications in spectroscopy and technology there is particular interest in analyzing the fundamental mechanisms responsible for the irreversible acceleration of electrons in fs laser-produced plasmas up to energies of many MeV and the subsequent photon generation [10,11]. Collective absorption processes, such as Brunel absorption and resonance absorption, become dominant for intensities above $I = 10^{16}$ W/cm^2. In a long scale preplasma, Raman instabilities, plasma wake-field acceleration, and relativistic self-focusing of the laser pulse also lead to suprathermal electron velocities [12].

Previous measurements of the hot electron temperature T_e in short pulse interactions indicate that one of several scaling laws may apply depending on the incidence angle and the density scale length [7]. For normally incident light, the "ponderomotive" scaling [13]

$$k_{\mathrm{B}}T_e \simeq 0.511 \ \mathrm{MeV}[(1 + I\lambda^2/1.37 \times 10^{18} \ \mathrm{W\,cm^{-2}\,\mu m^2})^{1/2} - 1]$$

(1)

has been verified for electrons directed along the target normal, exiting the rear side [1]. Obliquely incident light gives rise to a scaling $k_{\mathrm{B}}T_e \propto (I\lambda^2)^{1/3}$ associated with resonance absorption [14]. Shorter pulses and/or steeper gradients result in a similar scaling, but numerically lower values for T_e [10]. However, the total yield of electrons, photons, or secondary created particles depends on various experimental parameters such as target element, target surface properties, density scale length of plasma generated by laser prepulses, and, finally, laser polarization and direction of emission.

We demonstrate a novel method to simultaneously monitor spectrum and angular distribution over 2π of hard x-ray emission in absolute photon numbers from a femtosecond laser-produced plasma, generated with a laser intensity of 5×10^{18} W/cm^2 on the solid target. As a first application of these laser-produced MeV x rays, we released neutrons via a $^9\mathrm{Be}\,(\gamma, n)\,2\alpha$ reaction, demonstrating for the first time laser fission with a tabletop laser system.

The experiments described here were performed with the multi-TW Ti:sapphire laser system in Jena. The laser generates pulses of 60 fs duration, center wavelength of 800 nm, an energy of 250 mJ, and a repetition rate of 10 Hz. Two prepulses at 600 fs and 4 ps before the main laser pulse are known with relative intensities of 5×10^{-4} and 10^{-4} with respect to the main pulse. The range from 4 to 300 ps and from 2 ns on are prepulse free to a contrast ratio better than 10^5. The pulses are focused with a $f/2$ parabola to (4×7) μm^2, containing 50% of the energy. Incident angle on target is 45°, polarization parallel. The peak intensity on target is 5×10^{18} W/cm^2. The target is a 1.0 mm thick smoothed tantalum sheet ($Z = 73$). The target was moved between laser shots. For each run the radiation is accumulated over 20 000 shots.

The hard x-ray spectrum is measured with 12 spectrometers based on thermoluminescence detectors (TLD) [15,16]

(Fig. 1). Our spectrometers allow the absolute measurement of the photon fluence for photon energies between 10 keV and 2 MeV with a relative resolution of 20%. It was carefully verified that no scattered x rays excite the TLDs. No evidence of electrons penetrating through a 2 cm thick polymethylmethacrylate (PMMA) cover into the TLD stacks was found [17]. Contributions to the x-ray spectrum by bremsstrahlung generated in the PMMA were determined to be less than 15% by comparing the results from several TLDs equipped with front filters with either low or high Z materials, giving different radiation conversion coefficients.

Figure 2 displays two x-ray spectra detected by TLD spectrometers in the direction of specular reflection (solid circles) and in the forward direction with respect to the incident laser pulse (open squares). The absolute photon yield is given in number of photons per laser shot, keV, and sr. From the exponential decrease of the x-ray spectrum at high energies (solid line), we calculate a hot electron temperature T_e supposing bremsstrahlung from electrons with a Maxwellian energy distribution. Deconvolution of the TLD readings using a SAND II algorithm [15] yields $T_e \approx 700$ keV in the specular direction and $T_e \approx 300$ keV for the forward laser direction on the back side of the tantalum. The electron temperature is consistent with the ponderomotive scaling (see above), which predicts an electron temperature of 420 keV for a laser intensity of 5×10^{18} W/cm^2.

The photon flux scales nearly quadratically with the laser pulse energy: a 250 J shot in Livermore generated about 2×10^8 photons/(keV sr) at photon energy of 2 MeV which is 10^6 times times more than 200 photons/(keV sr) with our 250 mJ pulse [18]. And with a 25 J laser pulse 5×10^5 photons/(keV sr) at 2 MeV were counted in an experiment at the Rutherford Appleton Laboratory, which is again almost quadratic in energy [6].

Spectra similar to Fig. 2 were recorded in twelve directions within the plane of incident laser and target normal. Figure 3 shows the angular distribution of the *x-ray* temperatures retrieved from the high energy slope of the TLD spectrometer data (solid circles). The laser pulse impinges p polarized under 45° with respect to target normal. The maximum of about 500 keV is seen between the specular reflection and target front normal (330°), whereas in forward direction (215°) the temperature is only 200 keV.

Figure 4 displays the number of photons per keV, sr, and shot on a logarithmic scale as a function of the angle for three different photon energies: 488, 1160, and 1950 keV. Again, for energies above 500 keV the angular distribution is peaked on the front side of the target close to the specular direction.

The angle θ_e with which electrons are ejected from the target surface while the laser is incident can be found by momentum and energy conservation—analogously to free electrons ejected by a lateral ponderomotive force in an underdense plasma [19]. For the target geometry of Fig. 3, this is given by

$$\theta_e = 2\pi - \arctan\left\{ \frac{U\sin\theta}{\sqrt{2U + U^2\cos^2\theta}} \right\}, \qquad (2)$$

where $U = \gamma - 1 = E/mc^2$ is the normalized final kinetic energy of the electron and θ the incident angle. In the absence of scattering and self-induced fields, this result is independent of the acceleration mechanism. Similar expressions for oblique-incidence laser-solid geometry have been quoted by others [20]. The expression in Eq. (2) essentially says that the emission angle of electrons increases with kinetic energy, from $\theta_e = 0$ for $E \to 0$ up to $\theta_e = 2\pi - \theta$, the specular direction for $E \gg mc^2$.
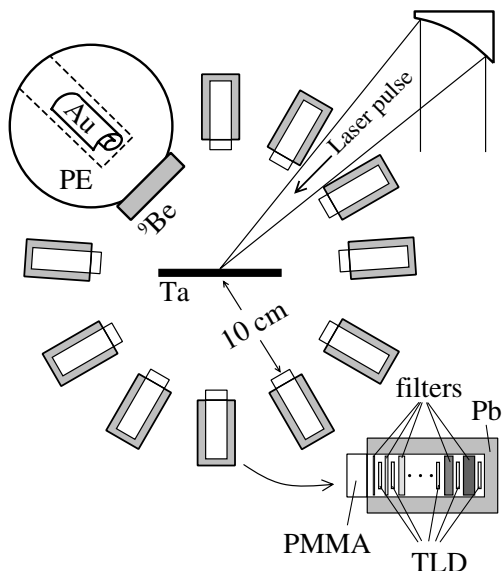

FIG. 1. Experimental setup for x-ray and photoneutron measurements. The inset shows the alternating arrangement of filters and TLDs in the x-ray spectrometers.
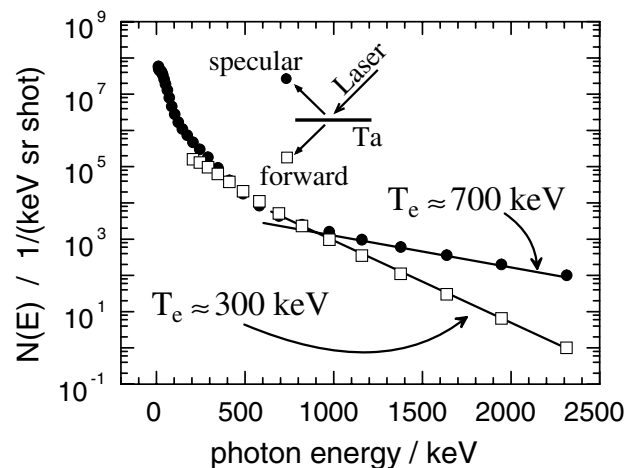

FIG. 2. Two characteristic x-ray spectra for different directions of emission, showing the deviation in hot electron temperatures.
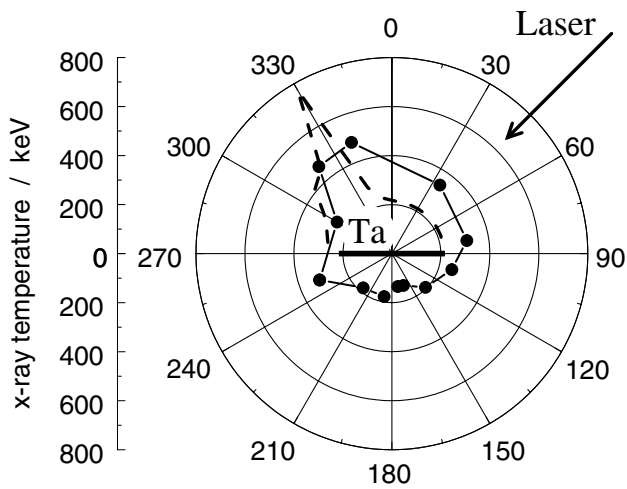
FIG. 3.   Angular dependence of the hot x-ray temperature. The circles are derived from the measured x-ray spectra. The dashed line shows the photon temperature due to a Maxwellian electron distribution of electrons ejected from the target surface (see text).

The angular distribution of the x rays points to some interesting features. Bremsstrahlung from weakly relativistic electrons ($E_\gamma < 0.5$ MeV) shows no significant deviation from isotropic emission. This may be attributed to multiple scattering of fast electrons in the target and the dipolar emission character of the bremsstrahlung. Therefore no direction is favored. This behavior changes distinctly for x-ray energies greater than the electron rest mass ($E_\gamma > 0.5$ MeV). Bremsstrahlung emission of electrons in this energy range is strongly peaked in the propagation direction of the electrons. This suggests that the detected angular distribution of MeV radiation resembles the distribution of the highly relativistic electrons. For the three energies in Fig. 4, Eq. (2) predicts emission angles of 325° (1950 keV), 329° (1160 keV), and 336° (488 keV), respectively, consistent with the observed x-ray emission peak of
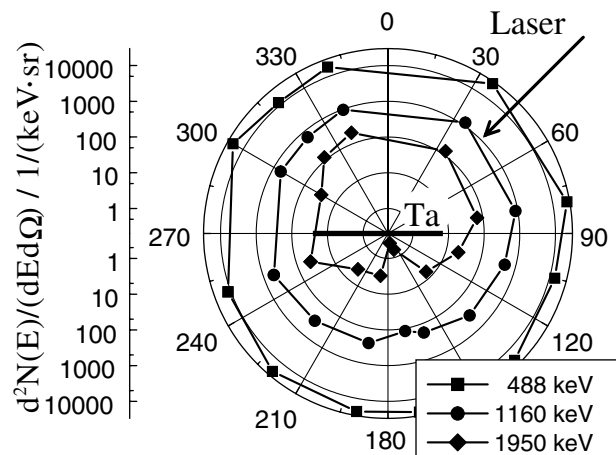

FIG. 4.   Angular distribution of the photon flux for three different photon energies. The logarithmic scaled plot shows a significant asymmetry for $E_\gamma > 500$ keV.

$(330 \pm 10)°$ for energies beyond 1 MeV. Our data therefore imply a jet of highly energetic electrons close to, but not exactly in, the specular reflection direction of the laser.

To analyze the data in Fig. 3 more fully, we suppose that a number of electrons are ejected from the target surface with a Maxwellian energy distribution $f(U) = T_e^{-1} \exp -U/T_e$. Combined with Eq. (2), this leads to an angular distribution $f(\theta_e)$ of emitted electrons, peaked near $\theta_e(T_e)$. To get the observed x-ray emission at a given detection angle, we sum the bremsstrahlung emission in the preplasma due to *all* electrons, weighted by $f(\theta_e)$ and taking into account the relativistic photon emission distribution [21]. The result is shown as the dashed line in Fig. 3 for an initial *electron* temperature of 300 keV. The broadening around the peak temperature exhibited by the experimental curve may be due either to an isotropic contribution from electrons in the target bulk, or to elastic scattering of electrons in the preplasma.

Assuming a 10% energy transfer from the laser pulse to suprathermal electrons, one finds that the plasma density in front of the target required to generate the measured x-ray yield in the specular direction is a few 10^{20} cm^{-3}, for a plasma volume of $(10 \ \mu m)^3$ given by the laser focus $\times$ the preplasma expansion within 100 ps. 10^{20} cm^{-3} is a realistic preplasma density generated with the unavoidable prepulse of multi-TW Ti:sapphire laser systems.

Electrons which are not reflected penetrate into the Ta bulk and generate bremsstrahlung. Some of these may also be scattered back out again (Molière scattering), particularly if they enter at the bulk with a finite angle [22]. The angular distribution of the bulk bremsstrahlung was calculated using a Monte Carlo model [23]. It contributes to the measured signal as an almost isotropic part.

In an experiment at the Rutherford Appleton Laboratory, Santala *et al.* observed anisotropic x-ray emission on the rear side of a thick tantalum target for photon energies above 10 MeV. The emission angle shifts from target normal (180° in the geometry of Fig. 3) to laser direction (225°) with increasing plasma scale length [7].

Kodama *et al.* [24] reported jets that give rise to x-ray emission in a substantial preformed plasma. They interpret their results using numerical simulations such that strong magnetic fields in connection with the specularly reflected laser light produce the electron jets. In our present experiments and complementary particle-in-cell simulations, a magnetic field is not required for directed electron emission and the direction of the electron emission is different from the specular direction.

Photonuclear reactions are widely used to characterize multi-MeV bremsstrahlung from conventional electron accelerators [25]. Very recently, (γ, n) reactions of several elements were successfully applied by both the Livermore and Rutherford Appleton Laboratories to characterize the bremsstrahlung spectrum of 1 PW and 100 TW laser-produced plasmas [16,18,26]. The applied intensities exceeded our values by factors of 100 and 10, the

deposited energies and the size of the laser system by 1000 and 100, respectively. However, the repetition rate is lower by a factor of 10 000 compared to our tabletop laser system.

Photons with energy above 1.67 MeV can disintegrate beryllium via a ^{9}Be $(\gamma, n) 2\alpha$ reaction. We placed a beryllium disk (12 mm thick, 70 mm diam) 4.5 cm away from the laser plasma in the specular direction of the incident laser, covering a solid angle of 1.3 sr (Fig. 1). The Be disk was wrapped in 60 μm thick aluminum foil and mounted on the surface of a polyethylene sphere (Bonner sphere) of 12.5 cm diameter [27]. About 40% of the neutrons generated in the Be disk enter the Bonner sphere and are thermalized by inelastic scattering with hydrogen and carbon. The neutron thermalization efficiency of the Bonner sphere was absolutely calibrated for the relevant neutron energies. A gold disk (^{197}Au, 16 g) was placed in the center of the Bonner sphere, capturing thermal neutrons ^{197}Au $+ n \rightarrow ^{198}$Au with a cross section of 99 b. ^{198}Au undergoes a beta decay with a lifetime of 2.7 d into ^{198}Hg promptly followed by emission of a 411.8 keV γ. The γ spectrum was collected by a Ge detector located 1 km below Earth for reduction of Au excitation by cosmic neutrons and low γ background [28].

In addition we placed several CR39 plastic nuclear track detectors around the tantalum target to monitor ions with energies $E > 100$ keV. None of the detectors showed protons with energies high enough to penetrate 60 μm of aluminum foil, which, in particular, excludes contribution from the ^{9}Be $(p, n)^9$B reaction to the neutron generation.

After 20 000 laser shots the activity of the ^{198}Au due to thermalized photoneutrons exceeded the natural background activation of gold by a factor of 2.5. This corresponds to about 100 photoneutrons per shot from the (γ, n) disintegration. *Fusion* neutrons were recently generated in two experiments elsewhere. Pretzler *et al.* generated 140 *fusion* neutrons per shot irradiating deuterated polyethylene target by a 2 TW laser [4]. Ditmire *et al.* counted 10^4 neutrons from deuterium *fusion* with a 100 mJ laser pulse into large D clusters [29].

From the number of neutrons generated in the beryllium disk one can infer the total number N_p of photons with energies larger than 1.67 MeV emitted from the relativistic plasma: Using an averaged photoneutron cross section of 0.5 mb above 1.67 MeV, we calculate $N_p = 3 \times 10^4$ (sr^{-1}), which corresponds well to the integrated photon yield of $N_{TLD} \approx 10^5$ (sr^{-1}) in the hot electron wing above 1.67 MeV which was achieved in the TLD measurement in the specular direction.

In conclusion, we measured for the first time the complete angular distribution of the hard x-ray spectrum of a relativistic, laser-produced plasma, generated on a tantalum surface with a light intensity of 5×10^{18} W/cm^2. We explained the strongly anisotropic x-ray emission charac-

teristics at relativistic photon energies by the bremsstrahlung generation of hot electrons ejected from the target surface and electrons penetrating into the bulk. Utilizing the detailed knowledge of the x-ray spectra we induced the photonuclear reaction ^{9}Be $+ \gamma \rightarrow 2\alpha + n$ by MeV photons from the laser-produced Ta plasma and demonstrated the neutron capture reaction ^{197}Au $+ n \rightarrow ^{198}$Au* with our compact laser neutron source.

[1] G. Malka and J. L. Miquel, Phys. Rev. Lett. **77**, 75 (1996).

[2] K. Krushelnick *et al.,* Phys. Rev. Lett. **83**, 737 (1999).

[3] E. L. Clark *et al.,* Phys. Rev. Lett. **84**, 670 (2000).

[4] G. Pretzler *et al.,* Phys. Rev. E **58**, 1165 (1998).

[5] M. D. Perry *et al.,* Rev. Sci. Instrum. **70**, 265 (1999).

[6] P. A. Norreys *et al.,* Phys. Plasmas **6**, 2150 (1999).

[7] M. I. K. Santala *et al.,* Phys. Rev. Lett. **84**, 1459 (2000).

[8] M. Tabak *et al.,* Phys. Plasmas **1**, 1626 (1994).

[9] H. Arnould *et al.,* Phys. Lett. B **458**, 167 (1999).

[10] P. Gibbon and E. Förster, Plasma Phys. Controlled Fusion **38**, 769 (1996).

[11] F. Brunel, Phys. Rev. Lett. **59**, 52 (1987); P. Mulser *et al.,* Laser Phys. **10**, 231 (2000).

[12] C. D. Decker *et al.,* Phys. Rev. E **50**, R3338 (1994); T. Tajima *et al.,* Phys. Rev. Lett. **43**, 267 (1979); A. Pukhov and J. Meyer-ter-Vehn, Phys. Plasmas **5**, 1880 (1998).

[13] S. C. Wilks *et al.,* Phys. Rev. Lett. **69**, 1383 (1992).

[14] F. N. Beg *et al.,* Phys. Plasmas **4**, 447 (1997).

[15] R. Nolte *et al.,* Radiat. Prot. Dosim. **84**, 367 (1999).

[16] M. H. Key *et al.,* Phys. Plasmas **5**, 1966 (1998).

[17] M. Schnürer *et al.,* Phys. Rev. E **61**, 4394 (2000).

[18] T. E. Cowan *et al.,* Phys. Rev. Lett. **84**, 903 (2000).

[19] C. I. Moore *et al.,* Phys. Rev. Lett. **74**, 2439 (1995).

[20] Y. Sentoku *et al.,* Phys. Plasmas **6**, 2855 (1999); H. Ruhl *et al.,* Phys. Rev. Lett. **82**, 743 (1999); A. A. Andreev *et al.,* JETP **89**, 632 (1999); Z.-M. Sheng *et al.,* Phys. Rev. Lett. **85**, 5340 (2000).

[21] B. K. Agarwal, *X-Ray Spectroscopy* (Springer, Heidelberg, 1991).

[22] H. Frank, Z. Naturforsch. **14A**, 247 (1959).

[23] D. C. Joy, *Monte Carlo Modelling for Electron Microscopy and Microanalysis* (Oxford University Press, Oxford, 1995).

[24] R. Kodama *et al.,* Phys. Rev. Lett. **84**, 674 (2000).

[25] J. J. Carroll *et al.,* Rev. Sci. Instrum. **64**, 2298 (1993).

[26] K. W. D. Ledingham *et al.,* Phys. Rev. Lett. **84**, 899 (2000).

[27] B. Wiegel *et al.,* Physikalisch-Technische Bundesanstalt Report No. PTB-N-21, 1994.

[28] S. Neumaier *et al.,* Appl. Radiat. Isot. **53**, 173 (2000).

[29] T. Ditmire *et al.,* Phys. Plasmas **7**, 1993 (2000).